Demonstration of the neutron tracking capability of NEXT in time-of-flight measurements to improve energy resolution

S. Neupane, ^{1,*} J. Heideman, ^{1,†} R. Grzywacz, ^{1,2} M. Cooper, ¹ J. Hooker, ¹ K.L. Jones, ¹ T.T. King, ^{1,‡} N. Kitamura, ¹ M. Madurga, ¹ K. Siegl, ¹ C.R. Thornsberry, ¹ P. Wagenknecht, ¹ Z. Xu, ¹ L.H. Heilbronn, ³ M.M. Rajabali, ⁴ A. Chester, ⁵ A. Richard, ^{5,§} Y. Alberty-Jones, ⁶ J. Derkin, ⁶ T.N. Massey, ⁶ D. Soltesz, ⁶ N. Brewer, ² B. Rasco, ² K. Rykaczewski, ² M. Wolinska-Cichocka, ⁷ and G. Savard ⁸

¹ Department of Physics and Astronomy, University of Tennessee, Knoxville, Tennessee 37996 USA

² Physics Division, Oak Ridge National Laboratory, Oak Ridge, Tennessee 37831 USA

³ Department of Nuclear Engineering, University of Tennessee, Knoxville, Tennessee 37996 USA

⁴ Department of Physics, Tennessee Technological University, Cookeville, Tennessee 38505 USA

⁵ Facility for Rare Isotope Beams, Michigan State University, East Lansing, Michigan 48824 USA

⁶ Department of Physics & Astronomy, Ohio University, Athens, Ohio 45701 USA

⁷ Heavy Ion Laboratory, University of Warsaw, PL 02-093 Warsaw Poland

⁸ Argonne National Laboratory, Lemont, Illinois 60439 USA

(Dated: August 31, 2022)

Precise neutron-energy measurements are required to probe the nuclear structure effects of neutron-rich nuclei, where β -delayed neutron emission becomes a dominant decay mode. The Neutron dEtector with Xn Tracking (NEXT) has been designed and constructed to measure β -delayed neutrons with better energy resolution. The new design localizes the neutron interaction position by optically segmenting the detector along the direction of the neutron flight path, reducing the associated uncertainties in the neutron TOF measurements. This significantly improves the energy resolution without losing the necessary detection efficiency. The proof-of-principle and efficiency measurements showed promising results. This article details the implementation of the neutron tracking capability of NEXT in time-of-flight measurements.

Keywords: Neutron emission, neutron detection, resolution

I. INTRODUCTION

New capabilities of the next generation radioactive ion beam facilities to produce very neutron-rich nuclei bring focus to neutron spectroscopy. Neutron spectroscopy is an important tool for obtaining the nuclear properties of the neutron-rich nuclei [1, 2] where β -delayed neutron (β n) emission is energetically favorable. The energy of the emitted neutrons can be determined using the time-of-flight (TOF) technique, where the energy resolution depends on the TOF resolution and the uncertainty in the flight path determination.

In this detection technique, the TOF is measured between a trigger detector, which provides the start time, and a neutron detector, which provides the stop time, over a specific flight path length. For a neutron detector with thick segments of plastic scintillator, the flight path depends on the scattering position as it traverses through the detector volume. High-resolution position determination is required to extract the proper flight path length. A new detector concept, Neutron detector with Xn Tracking (NEXT), was developed to constrain

NEXT is a plastic scintillator-based neutron TOF detector with the active scintillation volume optically segmented and coupled to position sensitive photomultiplier tubes (PMTs), allowing high-resolution timing and position measurements in β n spectroscopy. The precise timing and position measurements are equally crucial in reaction experiments for better angular resolution and precise Q value extraction. A full description of the NEXT concept, prototype design, detection efficiency, and data acquisition system can be found in the References [3, 4]. Here we present the advantages of NEXT's position localization in proof-of-principle measurements.

II. DETECTOR MODULES

A typical NEXT module has 8×4 optically separated segments of plastic scintillator, each with a cross-section of 12.7×6 mm² and 254 mm (10 inches) in length. During the prototyping phase, detector modules were also constructed with 5 and 20 inches long segments. Two different types of plastic scintillators from Eljen Technologies [5], EJ-276 and EJ-200, were used to construct the detector modules. EJ-276 has a neutron-gamma (n- γ) discrimination capability, while EJ-200 does not have any n- γ discrimination but has about 15% higher light yield than EJ-276. For conciseness, the modules are labeled based on the plastic type and length; for exam-

neutron scattering positions in the neutron TOF measurements.

^{*} sneupan4@vols.utk.edu

 $^{^\}dagger$ Now at Applied Research Associates Inc., Raleigh, North Carolina 27615 USA

 $^{^{\}ddagger}$ Now at Physics Division, Oak Ridge National Laboratory, Oak Ridge, Tennessee 37831 USA

[§] Now at Lawrence Livermore National Laboratory, Livermore, California 94551 USA

ple, EJ276-10 is constructed from EJ-276 plastic and is 10 inches long. The segmented plastic scintillator is coupled to a multi-anode photomultiplier tube (MAPMT) from Hamamatsu Photonics [6] on both sides for the light readout.

Each MAPMT provides 64 anode signals and one common dynode signal. Using the Anger logic and associated resistive readout board, we read only five signals; four anode signals for position analysis and a dynode signal for timing and pulse-shape analysis. The five signals from each Anger Logic board are recorded using 16-bit, 250 MHz Pixie-16 digitizers developed by XIA LLC [7]. The signal readout scheme of the NEXT is detailed in the Reference [4].

III. TOF CORRECTIONS

In the data analysis procedure, the detector response function is derived based on the neutron TOF, which also incorporates the spectrum's features due to scattering from the surrounding materials. The TOF spectrum is then deconvolved into neutron energies using the response function. This is a conventional procedure and relies on the fact that the neutron response function can be easier to characterize using TOF through measurements and simulations. The chosen procedure for the TOF correction in the following text is a consequence of this choice.

The neutron TOF spectrum should reflect measurements at a specific path length for precise energy determination. For this, the TOF must be corrected for the flight path length as it depends on the neutron interaction position in the detector volume. For this, the TOF is extracted for the original flight path and scaled to the fixed flight path for each event by,

$$t_0 = t \times \frac{L_0}{L},\tag{1}$$

where L_0 is the fixed flight path and L is the original flight path. If the TOF is scaled to the fixed flight path for each detector, the TOF for all detectors can be combined into a single spectrum and converted to an energy spectrum using a deconvolution procedure.

For a typical neutron TOF detector, the flight path length correction can be made only in one dimension, along the bar, which limits the detector's energy resolution. The distance along the detector axis is typically determined using time difference or light sharing between PMTs at opposite ends of the scintillator.

NEXT can localize the neutron interaction position in three dimensions in the detector, as shown schematically in Figure 1. This allows the scattering position to be corrected with greater precision, resulting in better energy resolution. The internal scattering position can be written into parallel and perpendicular components relative to a fixed flight path length. For NEXT,

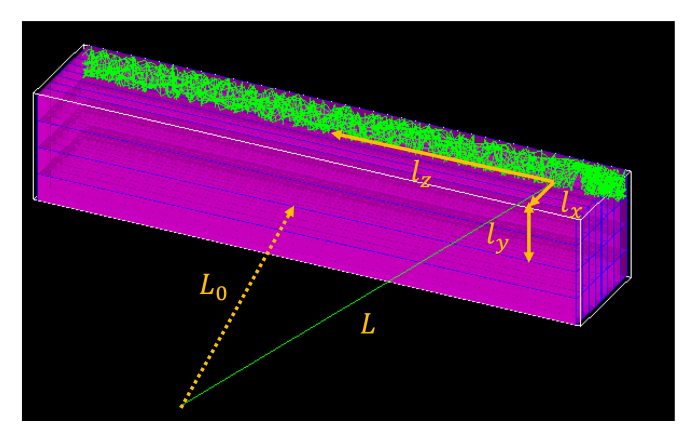


FIG. 1: The schematic demonstration of TOF correction procedure using the neutron interaction position inside the detector. Based on interaction position, the original flight path length (L) can be resolved into x, y, and z components with respect to a fixed flight path length (L_0) . The TOF is corrected for the flight path by scaling the actual TOF measurement by the ratio of L_0 and L.

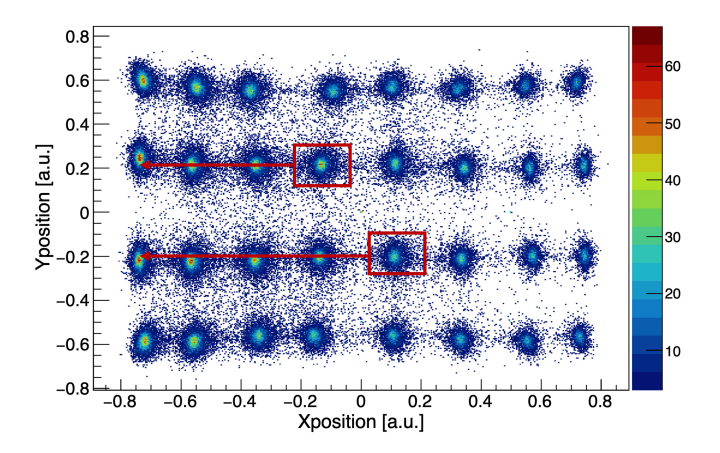


FIG. 2: The reconstructed neutron interaction position in the detector. The X and Y positions are the same as shown in Figure 1. The pixels represent the detector segmentation. The original TOF is obtained exclusively for each pixel and scaled to the middle of the first detector layer using Equation 1 as indicated by the red lines. See the text for the detail.

using the notations in Figure 1, L is then defined as $L = \sqrt{\left(L_0 + l_x\right)^2 + l_y^2 + l_z^2}$.

An example of the 2D reconstructed neutron scattering position (X and Y positions) in the detector obtained utilizing the four anode signals and the Anger logic algorithm [8] is shown in Figure 2. The pixels in Figure 2 are correspond to the detector segmentation. In the TOF correction process, pixels are defined by their physical size and position; the image in Figure 2 is used to identify which pixel the neutron interacted with. A group of pixels at the same X-position is referred to as a "column/layer," and the one at the same Y-position is referred to as a "row". The actual flight path length and corresponding TOF are determined exclusively for each pixel using this reconstructed position. The TOF is then scaled to the fixed flight path length, which is the middle

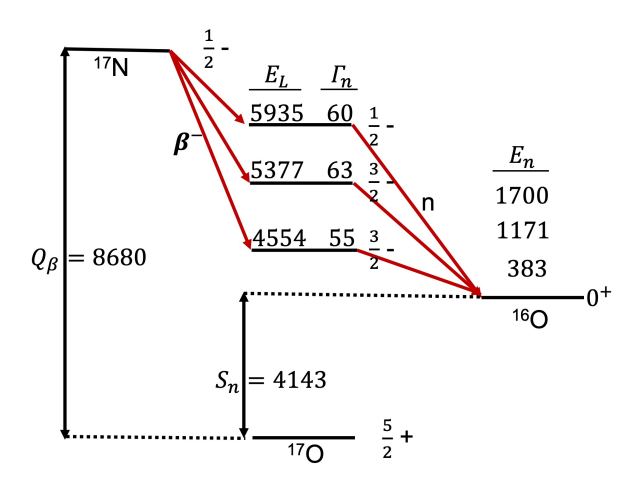


FIG. 3: The decay scheme of 17 N. The β -decay of 17 N populates the states above neutron separation energy in 17 O, which de-excite to the ground state of 16 O via neutron emission. All the energies are in keV.

of the first detector layer, using Equation 1, as shown graphically in Figure 2 by red lines.

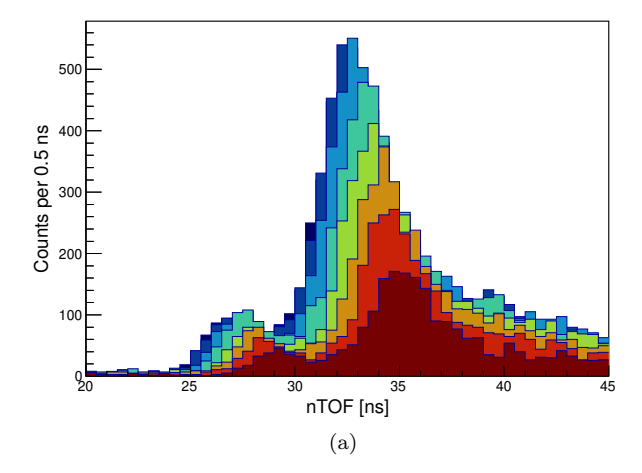
The following sections detail the TOF corrections using interaction position in the neutron TOF measurements. The term "uncorrected" refers to the TOF correction for the flight path is not implemented (treating as a typical non-segmented neutron detector), whereas "corrected" refers to the TOF correction implemented.

IV. 17 N β n EMISSION

The β -decay of ¹⁷N is well known for its subsequent neutron emission at energies of 383 keV, 1171 keV and 1700 keV, see Figure 3 [9, 10], which are suitable to characterize the NEXT array. The measurement was performed at National Superconducting Cyclotron Laboratory (NSCL) with an array of ten NEXT detectors: one EJ200-10, one EJ200-20, and the rest EJ276-10. NEXT modules were arranged in a circular arch with a flight path of \sim 50 cm from the ion implant position. Ions were implanted on Yttrium Orthosilicate (YSO) based segmented detector of dimensions $50.8 \times 50.8 \times 12.7$ mm³ [11], which also provided a start signal for the neutron TOF measurement.

The neutron TOF spectrum measured at individual detector layers (8 layers) is shown in Figure 4a, where a shift in the TOF centroid is observed with respect to the layer position. Once the TOF is corrected for flight path length using Equation 1, the TOF centroids lined up as seen in Figure 4b. Figure 5 shows the summed TOF spectra for all the layers without correction (black) and after correction (red). The TOF correction resulted in better-resolved peaks.

Another way of looking into the position-dependent timing is plotting the TOF against the neutron scattering position along the flight path direction (X-position).



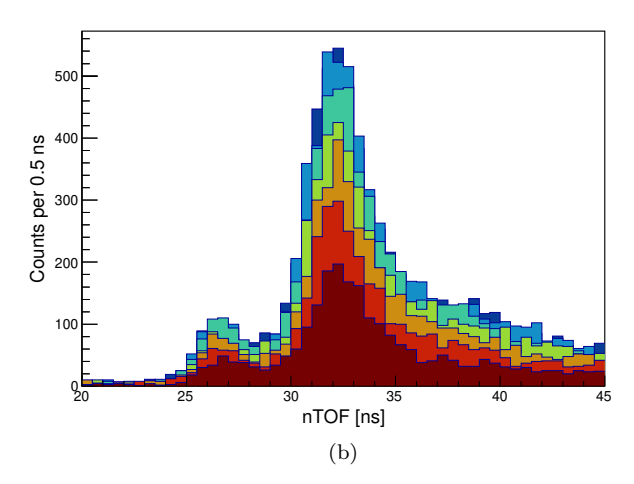


FIG. 4: The neutron TOF measured at the individual layers before the TOF correction (a) and after the TOF correction (b). The spectra are zoomed around two high-intensity peaks for clarity.

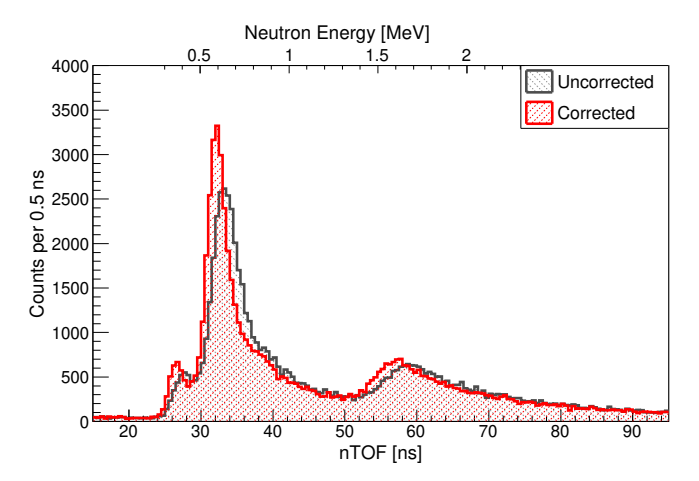
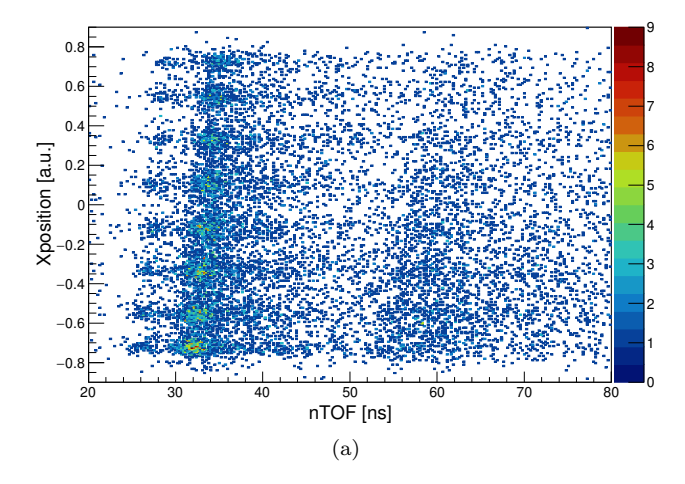


FIG. 5: The summed neutron TOF spectrum for ^{17}N β n emission before the TOF correction (black) and after TOF correction (red).

A linear relationship is observed between the TOF and scattering position for all three neutron groups with a slope depending on the neutron energy, as seen in Fig-



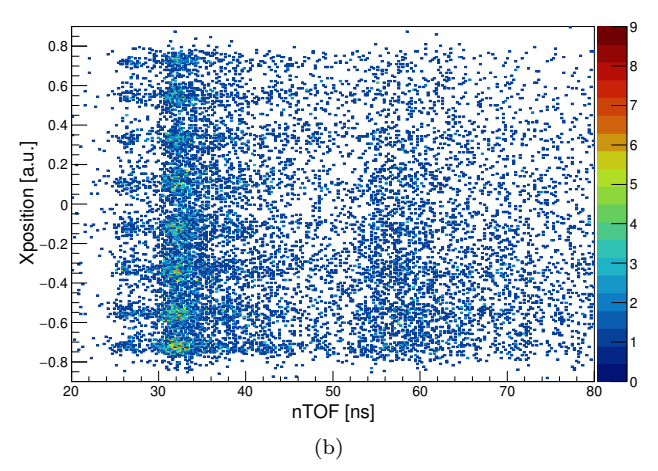


FIG. 6: The neutron TOF plotted against the interaction position along the flight path direction (X-position) for one of the NEXT detector modules before the TOF correction (a) and after the TOF correction (b).

ure 6a. This is translated into a poor separation between the TOF peaks, especially between the two high-energy peaks. After the correction, TOF becomes independent of the interaction position as shown in Figure 6b, resulting in better-separated peaks.

The neutron emitting states in ¹⁷O have non-negligible level widths [9] which are greater than the energy resolution of our detector. This added additional broadening in the neutron TOF peaks on top of our detector's resolution, ~700 ps from the implantation detector, and ~600 ps [3] from the NEXT. To see the effect of the level widths in the neutron TOF spectrum, simulation of the ¹⁷N neutron emission was performed using NEXTSim [3]. NEXTSim is a GEANT4-based simulation framework developed to characterize the NEXT detector units. NEXTSim was updated to incorporate the simulation of an array of NEXT modules mimicking the real experimental scenario. The same experimental setup used at NSCL was rendered in NEXTSim, and the three neutron energies, 383 keV, 1171 keV, and 1700 keV were simu-

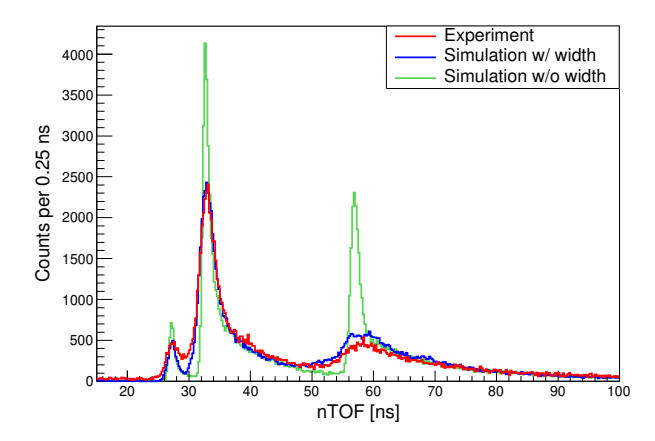


FIG. 7: The simulation of the 17 N neutron emission without widths (green) and with widths (blue) added to the neutron emitting states in 17 O, compared with the measured spectrum (red).

lated with and without level widths added. The level widths were taken from Reference [9]. The width of the neutron emitting states added a significant broadening to the neutron peaks, which can be seen in Figure 7.

Even though the energy resolution is limited by the timing resolution of the implant detector and the level width of the neutron emitting states, this measurement was successful in demonstrating the neutron interaction position localization capability of NEXT in real β n measurement.

V. ²⁷Al(d, n) THIN TARGET MEASUREMENT

Neutron detection efficiency of various NEXT prototypes was measured at Ohio University's Edwards Accelerator Laboratory (EAL), which provides neutrons with a wide energy distribution using $^{27}{\rm Al}({\rm d,n})$ reactions [16]. The key results from this measurement were reported in the Reference [4]. After the efficiency measurements were completed, an additional $^{27}{\rm Al}({\rm d,n})$ measurement was performed with a thin ($\sim\!50~\mu{\rm g/cm^2})$ $^{27}{\rm Al}$ target to test the energy resolution capability of NEXT. The 7.44 MeV deuteron beam impinging on a thin Al target allowed the measurement of well resolved high energy neutron peaks. A pickoff signal from the beam buncher was used as a reference signal for the neutron TOF measurements.

Two detector modules (EJ276-05 and EJ276-10) were stacked together to have better efficiency in detecting high-energy neutrons and placed at a distance of 5 m from the target assembly.

The raw TOF spectrum for stacked detectors without any correction made for internal scattering is shown in black in Figure 8. Using interaction position information, the TOF is corrected for flight path length using Equation 1. Once the correction is implemented, the peaks become better resolved, as shown in red in Fig-

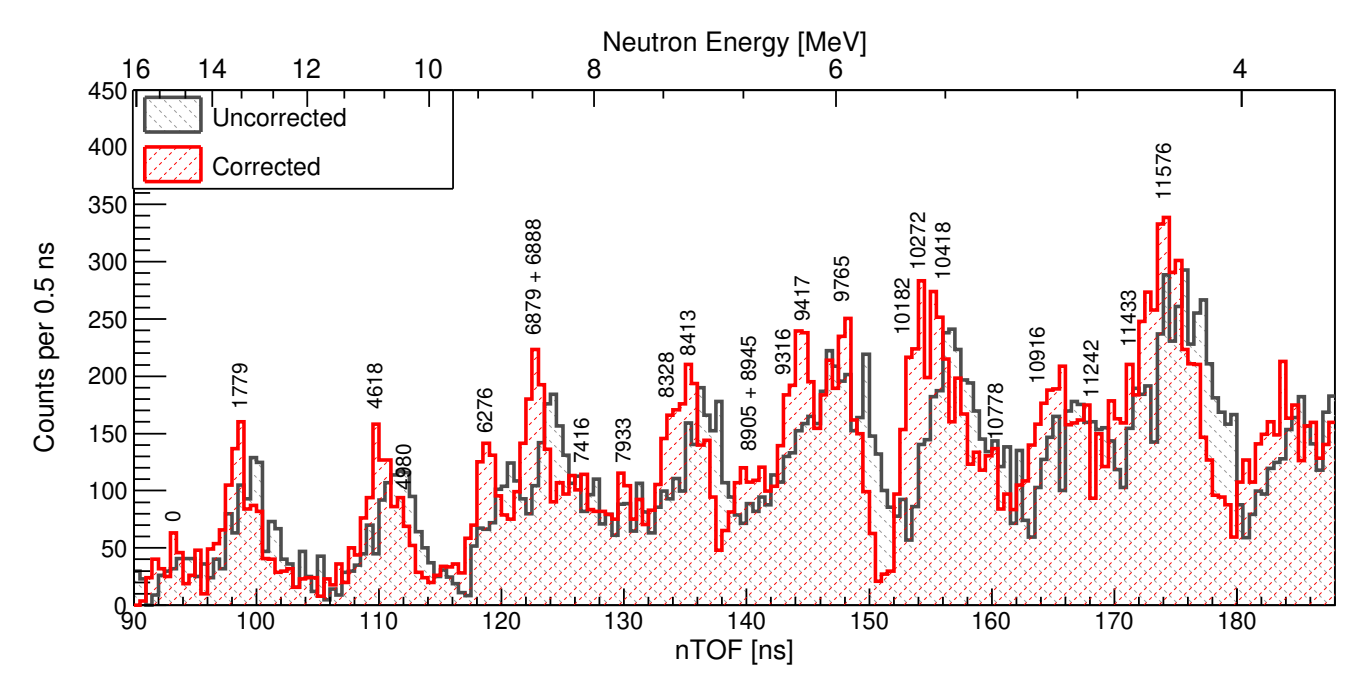


FIG. 8: The neutron TOF spectra for stacked detectors measured at EAL using 27 Al(d,n) reactions at 120° before the TOF correction (black) and after the TOF correction (red). The labels on the neutron peaks on the red histogram represent the corresponding excitation energies in keV in the residual nucleus 28 Si taken from previous 27 Al(d,n) and 27 Al(d,n) measurements [12–15].

ure 8, signifying the importance of the NEXT's neutron tracking capability in making more accurate and precise energy measurements. Here improvement in the energy resolution is limited by the timing resolution of the pick-off signal (\sim 1 ns) used as the start of the TOF and the short transit time (1-2 ns) for the neutrons to traverse the detector thickness.

VI. 106 Nb β n EMISSION

Another demonstration of NEXT's capabilities in β n measurement was carried out at the Argonne National Laboratory (ANL) using the beam from CARIBU Facility. The experiment took place at the focal plane of Modular Total Absorption Spectrometer (MTAS) [17]. As part of a survey of nuclei around ^{106}Mo , ^{106}Nb ($t_{1/2}=1.02~s, P_n=4.5\%$) ions were implanted on a tape system where the subsequent β n emission was observed from the neutron unbound states of ^{106}Mo . The allotted time for this isotope was only 8 hours.

A silicon photomultiplier (SiPM) based plastic scintillator detector was developed to detect beta decays and generate a start signal for neutron TOF measurements. The beta detector had to fit into a small space directly behind the tape implant point, so SiPMs were used because of their small form factor. Two 6x6 mm² Sensl J-Series SiPMs were mounted on a single readout board and coupled to a piece of the plastic scintillator (EJ-200). SiPMs are known for their characteristic dark counting, identical in shape to the pulse of detected photons. A coincidence between the two SiPM signals was required

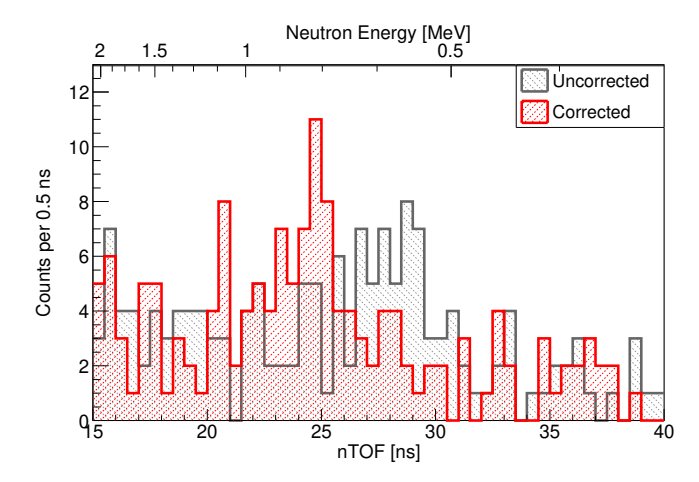


FIG. 9: The $^{106}\rm Nb$ neutron TOF spectrum before the TOF correction (black) and after the TOF correction (red). After the correction, a defined peak at ${\sim}760~\rm keV$ (25 ns) is observed. As the transit time for 760 keV neutron to traverse the detector thickness (${\sim}5~\rm cm)$ is about 4 ns a clear shift of 4 ns in TOF is seen after the correction in the 25 - 29 ns time range.

for a valid event in the analysis.

Five NEXT modules (four EJ276-10 and one EJ200-10) were installed with a $\sim \!\! 30$ cm flight path length around the implant position. The raw TOF spectrum for all modules combined without the TOF correction is shown in black in Figure 9. Once the TOF correction for flight path length was implemented using Equation 1, a clear neutron peak at $\sim \!\! 760$ keV above background was observed and shown in red in Figure 9. This first mea-

surement of $^{106}{\rm Nb}$ $\beta{\rm n}$ emission was important to show why a detector of this design is essential to the future study of neutron-rich nuclei. When isotope production and neutron branching ratios are not sufficient for the traditional neutron TOF detectors, NEXT can be easily adapted to provide a precise and efficient measurement.

tron energy resolution when a correction from the three-dimensional scattering position inside the detector is applied. The TOF correction procedure was benchmarked using $^{27}\mathrm{Al}(\mathrm{d,n})$ reactions and $^{17}\mathrm{N}$ $\beta\mathrm{n}$ emission and applied to the $^{106}\mathrm{Nb}$ decay, where it showed a dramatic change in the spectrum shape.

VII. CONCLUSION

As the capabilities of radioactive ion beam facilities are continually improving, the detector technology must also improve. NEXT is a novel neutron TOF detector for future studies of very neutron-rich nuclei. The position resolution provided by the segmentation in each detector module improves energy resolution in the neutron TOF measurements, which is vital to nuclear structure studies and astrophysics. NEXT is shown to improve neu-

ACKNOWLEDGMENTS

This work was supported by the U.S. Department of Energy, National Nuclear Security Administration under the Stewardship Science Academic Alliances program through DOE Award No. DENA0002934 and DE-NA0003899, an NSF Major Research Instrumentation Program Award Number 1919735. The Tennessee Technological University team was partially supported through grant No. DE-SC0016988.

- P. Dimitriou, I. Dillmann, B. Singh, V. Piksaikin, K. Rykaczewski, J. Tain, A. Algora, K. Banerjee, I. Borzov, D. Cano-Ott, et al., Nuclear Data Sheets 173, 144 (2021).
- [2] M. Pfützner, M. Karny, L. Grigorenko, and K. Riisager, Reviews of modern physics 84, 567 (2012).
- [3] J. Heideman, D. Pérez-Loureiro, R. Grzywacz, C. Thornsberry, J. Chan, L. Heilbronn, S. Neupane, K. Schmitt, M. Rajabali, A. Engelhardt, et al., Nuclear Instruments and Methods in Physics Research Section A: Accelerators, Spectrometers, Detectors and Associated Equipment 946, 162528 (2019).
- [4] S. Neupane, J. Heideman, R. Grzywacz, J. Hooker, K. Jones, N. Kitamura, C. Thornsberry, L. Heilbronn, M. Rajabali, Y. Alberty-Jones, J. Derkin, T. Massey, and D. Soltesz, Nuclear Instruments and Methods in Physics Research Section A: Accelerators, Spectrometers, Detectors and Associated Equipment, 165881 (2021).
- [5] Eljen technologies, https://eljentechnology.com.
- [6] Hamamatsu Photonics K. K., https://www.hamamatsu.com/jp/en/index.html.
- [7] XIA LLC, 2744 E 11th St, Oakland, CA, https://www.xia.com/.
- [8] H. O. Anger, J. Nucl. Med. 5, 515 (1964).
- [9] H. Ohm, W. Rudolph, and K.-L. Kratz, Nuclear Physics A 274, 45 (1976).
- [10] H. Miyatake, H. Ueno, Y. Yamamoto, N. Aoi, K. Asahi, E. Ideguchi, M. Ishihara, H. Izumi, T. Kishida, T. Kubo, et al., Physical Review C 67, 014306 (2003).

- [11] R. Yokoyama, M. Singh, R. Grzywacz, A. Keeler, T. King, J. Agramunt, N. Brewer, S. Go, J. Heideman, J. Liu, S. Nishimura, P. Parkhurst, V. Phong, M. Rajabali, B. Rasco, K. Rykaczewski, D. Stracener, J. Tain, A. Tolosa-Delgado, K. Vaigneur, and M. Wolińska-Cichocka, Nuclear Instruments and Methods in Physics Research Section A: Accelerators, Spectrometers, Detectors and Associated Equipment 937, 93 (2019).
- [12] J. Brenneisen, D. Grathwohl, M. Lickert, R. Ott, H. Ropke, J. Schmalzlin, P. Siedle, and B. H. Wildenthal, Z.Phys. A352, 149 (1995).
- [13] H. Satyanarayana, M. Ahmad, C. E. Brient, P. M. Egun, S. L. Graham, S. M. Grimes, and S. K. Saraf, Phys. Rev. C 32, 394 (1985).
- [14] W. Bohne, H. Fuchs, K. Grabisch, M. Hagen, H. Homeyer, U. Janetzki, H. Lettau, K. Maier, H. Morgenstern, P. Pietrzyk, G. Röschert, and J. Scheer, Nuclear Physics A 131, 273 (1969).
- [15] C. Miehé, A. Huck, G. Klotz, and G. Walter, Phys. Rev. C 15, 30 (1977).
- [16] T. Massey, S. Al-Quraishi, C. Brient, J. Guillemette, S. Grimes, D. Jacobs, J. O'Donnell, J. Oldendick, and R. Wheeler, Nuclear science and engineering 129, 175 (1998).
- [17] M. Karny, K. P. Rykaczewski, A. Fijałkowska, B. C. Rasco, M. Wolińska-Cichocka, R. Grzywacz, K. Goetz, D. Miller, and E. Zganjar, Nuclear Instruments and Methods in Physics Research Section A: Accelerators, Spectrometers, Detectors and Associated Equipment 836, 83 (2016).